

## OPTIMIZATION TOOLS IN THE ANALYSIS OF MICRO-TEXTURED LUBRICATED DEVICES

**Gustavo C. Buscaglia, Roberto F. Ausas**

Centro Atómico Bariloche and Instituto  
Balseiro  
8400 Bariloche, Argentina

**Mohammed Jai**

Centre de Mathématiques  
INSA de Lyon, CNRS-UMR 5585  
69621 Villeurbanne, France

### ABSTRACT

We address the problem of optimizing the performance of lubricated devices by means of artificial texturing. We consider a slider (or equivalently a thrust bearing) and minimize the friction using optimization tools such as sensitivity analysis and genetic algorithms. We show that textures that perform significantly better than the smooth (untextured) one can be found, and that the optimized texture depends on the working conditions (load, velocity). The GENESIS code that we used, with no fine tuning of algorithmic variables, proved a valuable tool in the identification of improved shapes.

### NOMENCLATURE

$h$	=	Local film thickness
$h_p$	=	Depth of dimples
$h_{\min}$	=	Minimum film thickness
$N_p$	=	Number of dimples
$N_g$	=	Number of groups of dimples
$a_c$	=	Square cell side
$a_p$	=	Edgelenlength of the dimples
$a_s$	=	Half distance between dimples
$k$	=	Steepness parameter
$x$	=	coordinate
$y$	=	coordinate across film thickness
$z$	=	coordinate
$p$	=	Local pressure
$U$	=	Velocity
$W$	=	Load capacity
$W_a$	=	Applied load
$F$	=	Friction force

### INTRODUCTION

Static and dynamic characteristics of lubricated devices are very sensitive to geometrical changes in the surfaces. The question then arises as to what improvements can be brought to, for example, a slider (which is also a model of a thrust bearing) by texturing its surface by some of the newly available methods such as indentation, chemical etching, laser ablation, etc. A few recent works have suggested that significant improvement can be brought to lubricated devices by artificial texturing [1, 2, 3].

This report addresses a preliminary study in this direction that makes use of optimization tools such as sensitivity analysis and genetic algorithms. We consider the simple case of a slider loaded with a static, vertical force. Only a texture on the static surface is considered, so that the texture distribution does not move with respect to the load and the problem has a time-independent steady state.

This simple case is important to understand the basic mechanisms that could bring improvement to the slider's performance. We study square texture cells with square microdimples, and optimize the dimples' size and depth.

The methodology is the solution of the Reynolds' equation by the Finite Element Method coupled to a Newton-like method to find the equilibrium position. At this position the relevant quantities, such as friction force and minimal film thickness, can be evaluated so as to drive the optimization algorithm.

The conclusions of this preliminary assessment are, basically, that optimization tools (either deterministic or stochastic ones) can indeed find improved designs of lubricated devices, even when the design variables are in fact at the micro-scale of the surface's texture. We considered it impor-

tant to assess evolutionary algorithms because in some areas of tribology the current trend is towards very sophisticated shapes that are not parameterized variations of previous ones. This article reports on a first step towards a systematic treatment of “optimum tribological surfaces”, or “engineered tribological surfaces”, by means of evolutionary algorithms.

## THEORY AND DEFINITIONS

### Governing Equation

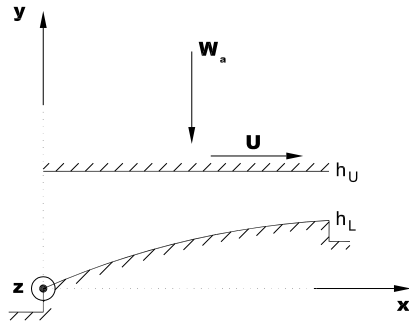


Figure 1: Schematic view of a slider.

The basic relation governing the slider lubrication problem is obtained by introducing the Reynolds assumptions into the Navier-Stokes equations. This relation (Reynolds equation) reads (see the coordinate system in Fig. 1):

$$\begin{cases} \frac{\partial}{\partial x}(h^3 \frac{\partial p}{\partial x}) + \frac{\partial}{\partial z}(h^3 \frac{\partial p}{\partial z}) = \frac{\partial h}{\partial x} & \text{in } \Omega \\ p = 0 & \text{in } \Gamma_D \\ \frac{\partial p}{\partial n} = 0 & \text{in } \Gamma_N \end{cases} \quad (1)$$

where  $\Omega$  is the integration domain and its boundary is defined as  $\partial\Omega = \Gamma_D \cup \Gamma_N$ , being  $\Gamma_D$  the Dirichlet part of the boundary and  $\Gamma_N$  the Neumann one.

We consider two geometries. The first one is periodic in the width direction, and thus models a slider of infinite width, while the second one corresponds to a finite-width slider with atmospheric pressure along the sides. The corresponding definitions are:

- **Infinite Width**

$$\begin{aligned} \Omega &= [0, 1] \times (-\frac{a_c}{2}, \frac{a_c}{2}) \\ \Gamma_N &= \{(x, z) \mid x \in [0, 1], z = \pm \frac{a_c}{2}\} \end{aligned}$$

- **Finite Width**

$$\begin{aligned} \Omega &= [0, 1] \times [0, B] \\ \Gamma_N &= \{(x, z) \mid x \in [0, 1], z = \frac{B}{2}\} \end{aligned}$$

where  $a_c$  is the square cell side and  $B$  is the slider width in the  $z$  direction.

The thickness of the fluid film can be expressed as:

$$h(x, z) = h_U - h_L + h_p \quad (2)$$

where  $h_U$  is the height of the upper surface, in which the load is applied,  $h_L$  is the height of the lower (textured) surface, but omitting the texture contribution (see Fig. 1), and  $h_p$  is the contribution to the fluid film thickness coming from the texture. In the case considered here  $h_U$  is the following quadratic function:

$$h_L(x, z) = 3x(2-x) \quad (3)$$

The equilibrium position  $h_U$  of the upper surface is found by Newton-Raphson iterations on the equilibrium condition

$$W(h_U) - W_a = 0 \quad (4)$$

where  $W_a$  is the applied load, assumed along the  $y$  direction, and

$$W = \int_{\Omega} p \, d\Omega \quad (5)$$

is the load capacity. The friction force  $F$  in the sliding direction ( $x$ ) is calculated by integrating the shear stress along the fluid film:

$$F = \int_{\Omega} \left\{ \frac{1}{h} + 3h \frac{\partial p}{\partial x} \right\} d\Omega \quad (6)$$

### Dimples

The dimples we consider are square and are arranged in a square pattern. They can be characterized by few parameters, as shown in Fig. 2. The edglength of the square cell than contains the dimple is denoted by  $a_c$ . The edglength of the dimple is  $a_p$ , so that the area fraction covered by dimples is simply  $\alpha = a_p^2/a_c^2$ . The third parameter that characterizes a dimple is  $h_{po}$ . In cell coordinates  $(\xi, \eta)$  the shape of the dimples is given by

$$\begin{cases} h_p = h_{p_o} \tanh \left[ k \sin \left( \frac{\pi(\xi - a_s)}{a_p} \right) \right] \times \\ \quad \tanh \left[ k \sin \left( \frac{\pi(\eta - a_s)}{a_p} \right) \right] & \text{if } (\xi, \eta) \in \Omega_o \\ h_p = 0 & \text{elsewhere in the cell} \end{cases} \quad (7)$$

where  $\Omega_o = [a_s, a_s + a_p] \times [a_s, a_s + a_p]$ ,  $a_s = \frac{1}{2}(a_c - a_p)$  and  $k$  is a “steepness parameter”.

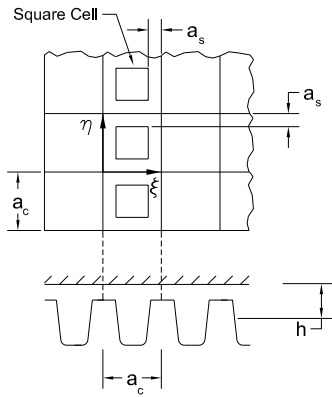


Figure 2: Schematic view of the dimples and an individual cell with its system of coordinates.

In the optimization process the domain  $\Omega$  is divided into regions. The dimples in each region are considered a “group”. The shape parameters ( $a_p$ ,  $h_{p_o}$  and  $k$ ) are varied keeping their values uniform for each group.

## Numerical formulation

The numerical treatment of Eq. (1) is a quite standard Galerkin finite element formulation. Considering a discrete space  $V_h$ , which satisfies the Dirichlet conditions, one looks for a pressure field  $p_h \in V_h$  satisfying

$$\int_{\Omega} \left[ h^3 \left( \frac{\partial p_h}{\partial x} \frac{\partial q_h}{\partial x} + \frac{\partial p_h}{\partial z} \frac{\partial q_h}{\partial z} \right) + h \frac{\partial q_h}{\partial x} + \frac{1}{\epsilon} |p_h^-| p_h q_h \right] dx dz = 0 \quad \forall q_h \in V_h \quad (8)$$

where  $p_h^- = \min\{p_h, 0\}$ , and  $\epsilon$  is the penalization parameter, that we take as  $10^{-10}$ . The term involving  $\epsilon$  models cavitation phenomena. In the

limit  $\epsilon \rightarrow 0$  it tends to satisfy the Elrod conditions  $p = \frac{\partial p}{\partial n} = 0$  at the boundary of the cavitation zone. The penalization is quadratic so as to render the left-hand side of (8) continuously differentiable with respect to  $p_h$ , which is convenient for the Newton-Raphson treatment of the nonlinearity. Though cavitation does not occur in the optimized shapes found in the cases reported here, it is important to include it because along the optimization process the evolutionary algorithms may propose shapes that produce cavitation.

## Optimization - Genetic algorithm

Code GENESIS Version 5.0 of J. Grefenstette (<http://www.aic.nrl.navy.mil/galist/src/#C>) was used as evolutionary algorithm in this study. A brief overview of the code is as follows:

Let  $f : R^n \rightarrow R$  be the objective function, and  $(X_1, X_2, \dots, X_n)$  its arguments (an  $n$ -vector). The algorithm works on a population (initially random)

$$P = \{(a_1, a_2, \dots, a_n), (b_1, b_2, \dots, b_n), \dots\} \quad (9)$$

making it evolve as shown in the diagram (see Fig. 3). Notice the classical steps in genetic algorithms[4]:

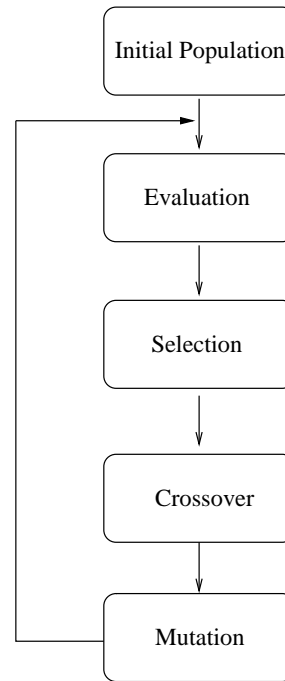


Figure 3: Flow chart of the genetic algorithm.

- *Evaluation*: Compute the objective function  $f$ . This is the most time-consuming step in our case since it involves a non-linear finite-element analysis.
- *Selection*: Randomly choose those individuals that survive to the next generation, assigning more probability to those with smaller  $f$ .
- *Crossover*: Randomly exchange genes (bits) between two individuals. The crossover rate can be controlled.
- *Mutation*: Randomly invert bits of an individual. The mutation rate can be controlled.

The GENESIS code allows for the mentioned rates and the population size to be adjusted so as have a reasonable convergence rate without saturation or instability.

## RESULTS AND DISCUSSION

### Rayleigh Step - Test case

As a first application a case with known optimum was chosen: The so-called Rayleigh step [5]. In this problem the objective function is the load capacity. The problem reads:

“Find  $h^*(x)$ ,  $h^*(x) \geq 1 \forall x \in [0, 1]$  such that

$$W[h^*] \geq W[h], \quad \forall h \quad (10)$$

where  $W[h]$  denotes the integral in (5) when  $p$  is the solution of (1). The exact optimum is given by (see Fig. 4):

$$\begin{cases} h(x) = 1 + \frac{\sqrt{3}}{2} & \text{if } x \in [0, \frac{1+2\sqrt{3}}{9}] \\ h(x) = 1 & \text{elsewhere} \end{cases} \quad (11)$$

The code GENESIS was used in three different ways. Notice that in this “validation” problem there are no dimples, we are simply optimizing the shape  $h(x)$  in the set of piecewise constants.

In *Case 1* the domain  $[0, 1]$  was divided into 100 subregions, the value of  $h$  in each subregion being a state variable. The variation range for each variable was set to be the interval  $[1, 2]$ .

In *Case 2* the subdivision was the same, but the first 65 variables were assigned the range  $[1.5, 2]$ , the following 10 variables the range  $[1, 2]$  and the remaining 25 variables the range  $[1, 1.5]$ .

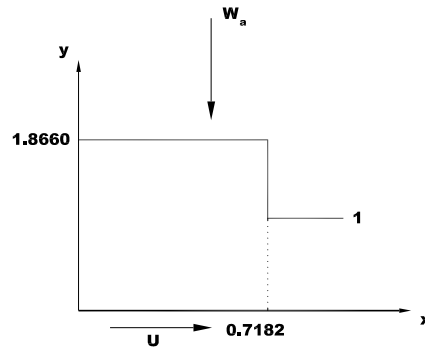


Figure 4: Non-dimensional Rayleigh step.

Finally, in *Case 3* it was assumed that the profile had stepped shape. The state variables were, thus, the film thickness on the left of the step,  $h_{left}$ , the film thickness on the right,  $h_{right}$ , and the discontinuity location,  $D$ .

The results from the first two cases after 30,000 evaluations of the objective function can be seen in Fig. 5, compared to the exact optimum. Results from *Case 3* can be observed in Table 1, as a function of the number of evaluations. The load value obtained for *Case 1*, corresponding to the shape shown in Fig. 5, is 0.9789 of the exact optimum, while that of *Case 2* is 0.9921 of the exact optimum. In these cases a population size of 50 individuals was taken.

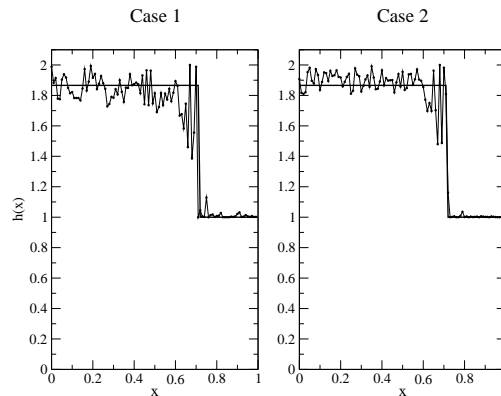


Figure 5: Results of the GENESIS code compared to the optimal Rayleigh step. Left: *Case 1*, Right: *Case 2*.

The mutation and crossover rates used in the

calculations were 0.001 and 0.6 respectively.

Table 1: Results of the GENESIS code compared to the exact ones, indicating the number of evaluations (*Case 3*).

<i>Parameter</i>	$h_{left}$	$h_{right}$	$D$
<i>Exact</i>	1.8660	1	0.7182
100 <i>Eval.</i>	1.8756	1.00044	0.7029
500 <i>Eval.</i>	1.8662	1.00048	0.7029
4000 <i>Eval.</i>	1.8662	1.00039	0.7154
10000 <i>Eval.</i>	1.8662	1	0.7174

The above results show that in general the genetic algorithm leads to “rough” shapes, especially in regions where  $h$  is much greater than one. The lubrication equation is not very sensitive to changes in the film thickness at regions where this thickness is large. Since the “rough” shapes have loads very close to the optimal one, no driving force exists for smoothing out the shape. Of course, if the algorithm is allowed to proceed indefinitely, the exact shape is eventually attained. For *Case 2* above this happens after 200,000 function evaluations, approximately, and only then the obtained shape is “smooth”. It could be interesting to design a smoothing procedure specific for partially-optimized lubrication shapes. It has also been shown that adding information, as is expected, narrows the state space and allows the algorithm to get close to the optimum in fewer generations.

Another interesting point is the algorithm’s behavior as a function of the number of state variables. In Table 2 we show the best load value (relative to the optimal one) as attained after 30,000 evaluations of the cost function. Compare the results with different numbers of state variables  $N_{var} = 50, 100$  and 200. It is clear that the fewer the state variables, the fewer the number of iterations to get to within some given tolerance from the optimum. In all three cases of Table 2 the ranges of the variables were set according to *Case 2* described above.

Finally, let us briefly comment about algorithmic parameters. The GENESIS code has default values for the crossover and mutation rate constants. Varying any of these constants does not have an impact on the convergence behavior of the algorithm. An example is shown in Figs. 6-8, in which the mutation rate constant is varied keeping the crossover rate constant fixed. It is observed that

Table 2: Relative Load Capacity obtained with the GENESIS code using 50, 100 and 200 variables to define the film thickness  $h$ .

$N_{var}$	<i>Relative Load Capacity</i>
50	0.9991
100	0.9921
200	0.9629

increasing the mutation rate constant by an order of magnitude does not affect the convergence behavior of the algorithm significantly. Only after setting the constant to 100 times the default value (Fig. 8) the mutation inhibits convergence.

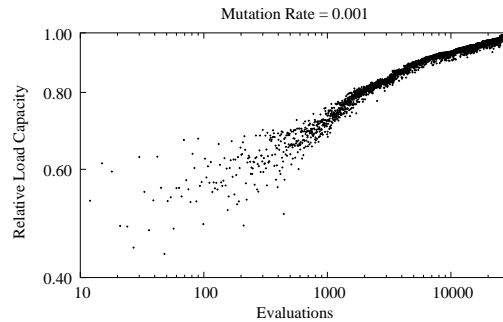


Figure 6: History of the objective function along algorithmic iterations (relative to the exact optimum). The mutation rate constant is set to the default value of the GENESIS code, 0.001. The ticks in the vertical axis have a spacing of 0.1.

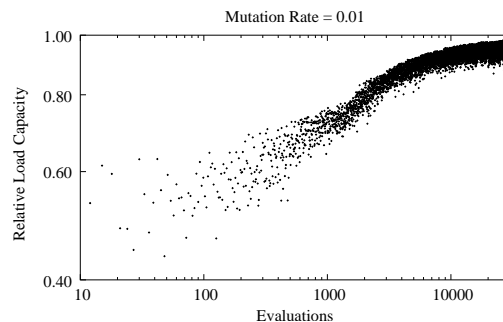


Figure 7: History of the objective function along algorithmic iterations (relative to the exact optimum). The mutation rate constant is set to 0.01.

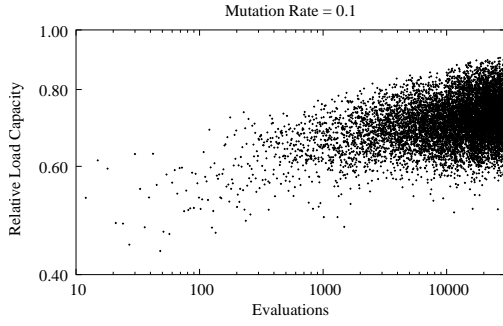


Figure 8: History of the objective function along algorithmic iterations (relative to the exact optimum). The mutation rate constant is set to 0.1, a value that is too high to attain convergence.

## TEXTURED SLIDERS

Going now to the technological problem of texture design in the slider configuration (Fig. 1), in this case the objective function is  $f = F$ , the friction force, while the state variables  $\{X_j\}$  are texture-shape coefficients.

### Infinite width case

We consider a square array of dimples, periodic in the width ( $z$ ) direction. We first conducted a sensitivity analysis in order to narrow the search space, studying the variations of the friction and of the minimal spacing *around the untextured state* ( $h_{po} = 0$  everywhere) with respect to dimple depth.

Let  $h_{po}^I$  denote the value of  $h_{po}$  for the  $I$ -th group of dimples. Since all other input data are fixed, the solution of the problem (i.e., the pressure field, the excentricity, the minimal film thickness, the friction force, etc.) depends just on  $\{h_{po}^I\}_{I=1, \dots, N_g}$ . We can thus calculate derivatives of any quantity, such as for example the friction force  $F$ , by numerical differentiation, that is

$$\frac{\partial F}{\partial h_{po}^I} \left( \bar{h}_{po}^1, \dots, \bar{h}_{po}^I, \dots \right) = \frac{F(\bar{h}_{po}^1, \dots, \bar{h}_{po}^I + \delta, \dots) - F(\bar{h}_{po}^1, \dots, \bar{h}_{po}^I, \dots)}{\delta} + \mathcal{O}(\delta) \quad (12)$$

Whether it is convenient or not to carve dimples in some region of the bearing results from the derivative of  $F$  and  $h_{min}$  with respect to  $h_{po}^J$ . These derivatives are shown in Fig. 9. Based on

them, we consider the following dimple-depth distribution:

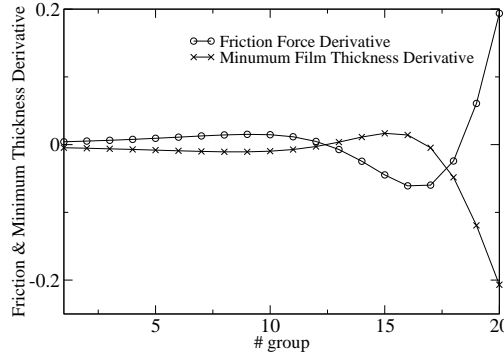


Figure 9: Friction Force and Minimum Film Thickness Derivatives along the slider.

$$h_{po}^J \begin{cases} \neq 0 & \text{if } \frac{\partial F}{\partial h_{po}^J}(0) < 0 \quad \text{and} \quad \frac{\partial h_{min}}{\partial h_{po}^J}(0) > 0 \\ = 0 & \text{in any other case} \end{cases} \quad (13)$$

so as to allow dimples only where  $F$  is expected to decrease while  $h_{min}$  is expected to increase.

The dimple width is set to  $1/100$ , and the domain is divided into  $N_g = 20$  subregions, so that each subregion contains a group of 5 dimples. From criterion (13) the search space is narrowed to groups 12 to 17. In these groups we set as variables the dimple depth  $h_{po}$ , width  $a_s$ , and the steepness parameter  $k$ , within the ranges

$$h_{po} \in [0, 1.4] - a_s \in [0.0008, 0.0025] - k \in [2.5, 5]$$

The total number of variables is thus 18.

The evolution of the friction and of  $h_{min}$  along the evolution process is shown in Fig. 10 for a non-dimensional applied load of 0.06. Notice that the results are shown relative to the smooth case. A significant improvement of 4 % is obtained. Moreover, this improvement comes with a 2 % increase in the film thickness, which is important in terms of wear. The texture corresponding to the best individual found can be seen in Fig. 11. Also shown in the figure is the optimized shape corresponding to a smaller applied load,  $W = 0.006$ . It is clear that the optimized textures strongly depend on the operating conditions of the device.

### Finite width case

In this case we simulate half the width of the slider because of the symmetry. The cell width

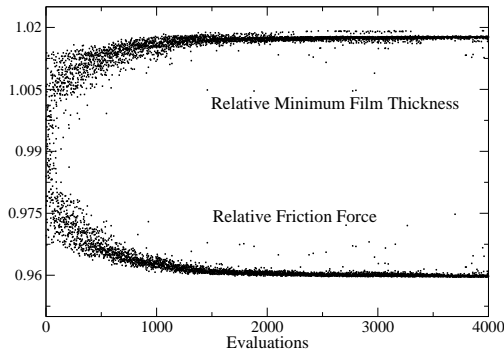


Figure 10: Relative Friction Force and Minimum Film Thickness. Evolution along the optimization process. Notice that a 4% decrease in Friction, together with a 2% increase in Minimum Film Thickness, is attained.

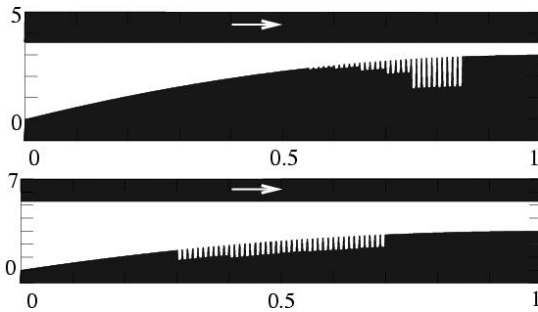


Figure 11: Optimized textures for two different non-dimensional loads: 0.06 (top) and 0.006 (bottom).

adopted is  $\frac{1}{24}$ , so that the maximum number of dimples is  $288 = 24 \times 12$ . Dimples are only allowed in the central portion of the slider (see Fig. 12), since from the previous paragraph we know that this portion is the one in which dimples can be beneficial.

In Fig. 13 we illustrate the pressure field corresponding to a uniform dimple depth of  $h_p = 0.5$ . The dimples were divided into 35 groups of  $2 \times 2$  dimples each. Two free parameters were assigned to each group of dimples, the depth and the size, with the ranges:  $h_{po} \in [0, 1.3]$  -  $a_s \in [0.0025, 0.007]$ .

The total number of parameters is thus 70. Again the genetic algorithm found a design with a 4.7 % reduction in friction force. The best texture found after 3000 evaluations of the objective function is shown in Fig. 14.

The result after 18000 evaluations is given in Figs. 15 and 16. The reduction in friction force cor-

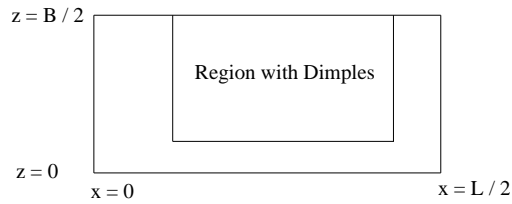


Figure 12: Scheme showing the region in which dimples are introduced in the finite-width case.

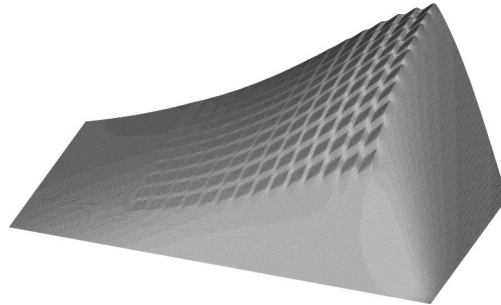


Figure 13: Pressure distribution when a uniform texture is introduced in the region indicated in Fig. 12

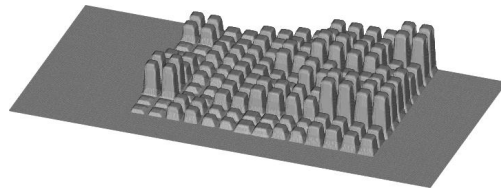


Figure 14: A 3D view of depth distribution of the optimized texture obtained after 3000 evaluations of the objective function. The maximum depth is 1.292, the minimum one is 0.085.

responding to this pseudo-optimal texture is 5.2 %.

## CONCLUSIONS

The recent development of advanced surface texturing techniques, such as laser ablation, chemical etching, etc., opens the possibility of “engineered surfaces” for lubrication devices [2, 3]. There exists significant activity in this direction, since important gain can be achieved in terms of friction, wear and lifetime extension.

It should not however be believed that some magical texture exists that is optimal no matter what the load and velocity of the device is. For each specific working condition there exists a spe-

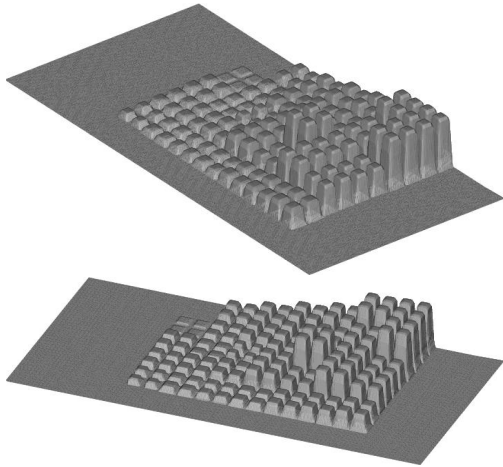


Figure 15: Two 3D views of depth distribution of the optimized texture obtained after 18000 evaluations of the objective function. The maximum depth is 1.294, the minimum one is 0.0025.

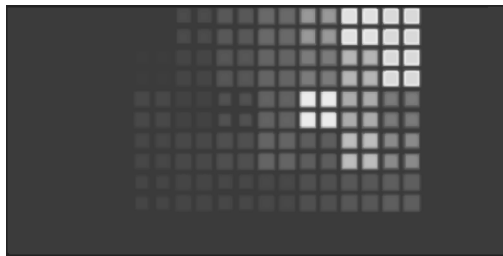


Figure 16: Optimized texture with the depth shown by means of color zones. The maximum depth is 1.294 (brighter), the minimum one is 0.0025 (darker).

cific texture that improves the performance, but it depends on the load and velocity. Optimal design is necessary to identify the surface shape that is best suited for each device. It is thus appropriate to assess different optimization tools in this problem.

In this article we have focused on evolutionary algorithms, which have the potential of identifying global optima, and the results have shown that quite standard genetic procedures work rather well for the problem under study. Further investigation is however required since the cases considered do not involve crucial phenomena such as massive cavitation and viscous heating.

Notice, to conclude, that we have assumed throughout this analysis that the Reynolds approximation holds. This requires that the length scales in the sliding direction are much greater than the

dimple depth. If the dimple length is comparable to its depth, the Navier-Stokes equations need to be solved to calculate the effect of the dimples and eventually optimize the design. This is the subject of ongoing research.

## Acknowledgments

The authors acknowledge support from Agencia Nacional de Promoción Científica y Tecnológica (Argentina) through grants PICT'99 12-6337 and PICT'00 12-9848.

## REFERENCES

- [1] A. Ronen, I. Etsion and Y. Kligerman, Friction-reducing surface-texturing in reciprocating automotive components, *Tribol. Trans.*, **44**, 359–366 (2001).
- [2] I. Etsion and G. Halperin, A laser surface textured hydrostatic mechanical seal, *Tribol. Trans.*, **45**, 430–434 (2002).
- [3] G. Ryk, Y. Kligerman and I. Etsion, Experimental investigation of laser surface texturing for reciprocating automotive components, *Tribol. Trans.*, **45**, 444–449 (2002).
- [4] D.T.Pham and D. Karaboga. *Intelligent Optimization Techniques - Genetic Algorithms, Tabu Search, Simulated Annealing and Neural Networks*, Springer.
- [5] L. Rayleigh. *Notes on the Theory of Lubrication*, *Philosophical Magazine*, 35:1-12, 1918